DOI 10.1515/aot-2013-0025 — Adv. Opt. Techn. 2013; 2(4): 323–329

Research Article

Pablo Benitez*, Juan C. Miñano, Julio Chaves and Asunción Santamaría

SMS freeforms for illumination

Abstract: SMS 3D (simultaneous multiple surfaces in their three-dimensional version) is a well-known design method comprising two freeform surfaces that allow the perfect coupling of two wavefronts with another two. The design algorithm provides a collection of line pairs on both surfaces (called SMS spines), whose three-dimensional shape seems arbitrary at first sight. This paper shows that the shapes of the spines are partially governed by applying the étendue conservation theorem to the biparametric bundle of rays linking the paired spines, which is one lesser known étendue invariants found by Poincaré. The resulting formulae for the spines in three-dimensional space happen to coincide with the conventional étendue formulas of two-dimensional geometry, like for instance, the Hottel formula.

Keywords: étendue; freeform; optical design; SMS.

OCIS codes: 230.0230; 080.2175; 080.4298.

***Corresponding author: Pablo Benitez,** Technical University of Madrid, Campus de Montegancedo, 28223, Pozuelo, Madrid, Spain; and LPI, 2400 Lincoln Avenue, Altadena, CA 91001, USA, e-mail: pablo.benitez@upm.es
Juan C. Miñano: Technical University of Madrid, Campus de Montegancedo, 28223, Pozuelo, Madrid, Spain; and LPI, 2400 Lincoln Avenue, Altadena, CA 91001, USA
Julio Chaves: LPI, 2400 Lincoln Avenue, Altadena, CA 91001, USA
Asunción Santamaría: Technical University of Madrid, Campus de Montegancedo, 28223, Pozuelo, Madrid, Spain

1 Introduction

Rotationally symmetric optics cannot satisfactorily solve some non-symmetric design problems in illumination. Typical examples of these cases are automotive low-beam headlights solar concentrators and street lights. In these cases, sources and targets usually have very asymmetric requirements. A rotational symmetric optical device can partially solve the problem, particularly if we relax conditions on the efficiency of light transfer and on the number of elements that make up the optical system.

Freeform surfaces provide additional degrees of freedom which may be used to solve asymmetric problems more satisfactorily, with higher efficiency or a fewer elements at the expense of tooling freeform surfaces, which are more difficult than rotational or linear symmetric ones. However, this extra cost is rapidly paid back through mass production in most cases.

Design procedures for freeform optical devices have not evolved as fast as tooling [1, 2]. Essentially, there are two strategies for optical design methods: numerical optimization [3–6] and direct methods.

A direct method is a mathematical procedure which delivers the optical surface equations without iterations when the optical prescription is given, as opposed to optimization, in which a sequence of optical surfaces is obtained in iterations.

There are basically three direct design methods for freeform surfaces in nonimaging optics: Monge-Ampere type partial differential equations [7–9], generalized Cartesian ovals, and the simultaneous multiple surfaces in their three-dimensional version (SMS 3D) [10]. The Monge-Ampere equations and Cartesian ovals solve their design problems exactly only for point sources, whereas SMS deals with the extended ones. Significant progress is being made in the Monge-Ampere case to generalize it to an extended source, using iterative compensation algorithms [11].

A generalized Cartesian oval is an optical surface which makes the optical path length between two prescribed wavefronts constant. The optical prescription is given by these two wavefronts. Descartes was the first to design using this procedure but restricted it to spherical wavefronts. The resulting surfaces are called Cartesian ovals (they are named after him) are not freeform (strictly speaking) but aspherics [12, 13]. When the optical surface is a reflector, the Cartesian ovals obtained from spherical wavefronts are quadrics. Levi-Civitta generalized the problem to non-spherical wavefronts. In this case, the resulting optical surfaces are, in general, freeform [14].

The SMS 3D design method can be seen as one step ahead of the Cartesian oval problem [15]. To design an optical system that perfectly couples two input wavefronts into two output wavefronts, it turns out that two freeform

surfaces are in general sufficient for the optical system to solve the problem. The optical prescription is given by the sets of input and output wavefronts. The resulting optical surfaces have no analytical expression and must be calculated simultaneously point by point. The coupling of a greater number of wavefronts even with only two surfaces is also possible when the rays of the design wavefronts cross only a fraction of the surfaces [16].

In this paper, we will focus on some new aspects of the SMS 3D method related to the étendue conservation of two-dimensional (2D) ray bundles inherent in the design process. One of the interesting aspects of the SMS freeforms is that they can be not only designed for nonimaging applications but also for imaging applications [17]. However, the imaging SMS is outside of the scope of this paper.

2 The SMS 3D design method

Let us consider an asymmetric mirror lens concentrator, known as XR in the SMS nomenclature, shown in Figure 1 as an example of SMS design in which the two surfaces are a mirror and a single-sided lens. Such a device has been applied for both photovoltaic applications [18] and (reversed) for automotive LED lighting [19]. Seen in the photovoltaic mode, the two input wavefronts that will be perfectly coupled with the SMS method are the plane wavefronts whose rays will be impinging on the mirror and are perpendicular to the red and blue directions of the direction cosine p-q plane, as detailed in Figure 1. These wavefronts will be coupled to the spherical wavefronts converging on the respective blue and red points on the edge of the solar cell in Figure 1, and these rays are called edge rays in the nonimaging optics nomenclature.

In the Cartesian oval problem, once the refractive indices are given, the boundary condition is just one point on the surface. However, in the SMS 3D, the boundary condition is a full line in 3D space contained in one of the surfaces and the normal vectors to the surface along the line, and the length of the optical path between one of the wavefront pairs. This line is called a seed rib in SMS nomenclature, and can be selected to couple with another two wavefront pairs along it also using the SMS. In the case detailed in Figure 1, these wavefronts are also selected as those associated with the edge rays in the green and pink colors, and then the SMS lines are contained in the plane of the y-z symmetry and are shown in Figure 2. Any of these two lines can be used as the seed rib for the following SMS 3D construction.

From each point of the seed rib, the SMS design method applied to the red and blue wavefronts provides a succession of isolated points on both surfaces, called an SMS chain. After a smooth interpolation between two adjacent points of an SMS chain, the SMS method can be applied to join the isolated points creating the SMS spines, which are rather transversal to the seed rib (Figure 3). Therefore, the procedure guarantees the perfect coupling of the blue and red wavefronts, whereas the pink and green wavefronts are only perfectly coupled along the seed rib in the symmetry plane.

3 Understanding the SMS freeform shapes

The shape of the freeform mirror in Figure 1 is not too far from an axisymmetric off-axis paraboloid, because the reflected rays are concentrated onto the rather small surface of the lens. However, it is interesting to take a detailed look at the very unusual shape of the freeform surface of the lens, as shown in Figure 4.

To understand the shape of the freeform lens, it is useful to consider first the comparison between the two

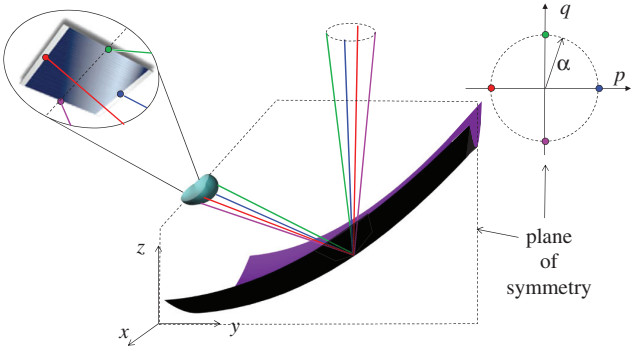

Figure 1 XR SMS 3D freeform photovoltaic concentrator.

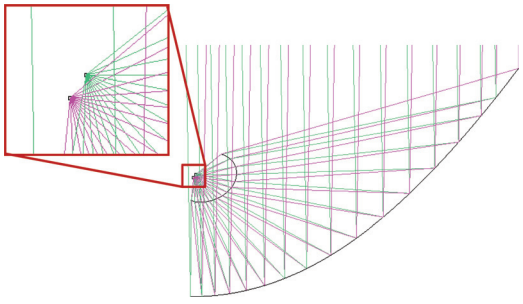

Figure 2 SMS seed ribs calculated in the plane of symmetry of the XR in Figure 1 using the green and pink wavefronts and rays.

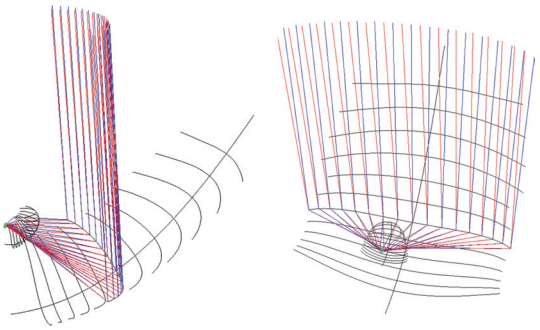

Figure 3 Two perspective views of the SMS spines lying on the seed ribs calculated using the blue and red wavefronts and rays.

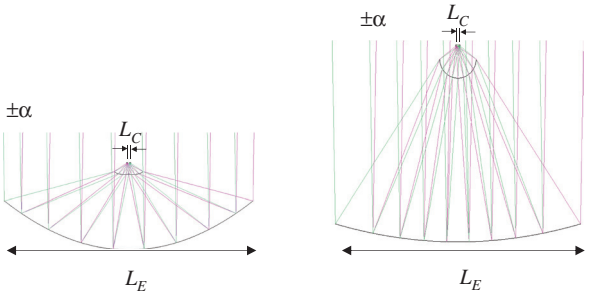

Figure 5 Two XR designs in 2D with the same entry and receiver sizes (L_E and L_C) and the same acceptance angles α but very different separation between the mirror and the lens vertices.

symmetric XR designs in 2D shown in Figure 5. Both designs have the same design parameters L_E, L_C and α, that is, both are designed to transfer perfectly the biparametric input bundle impinging on the mirror length L_E with an angle with the vertical small or equal to α onto the cell of length L_C. However, the two designs differ in the distances from the mirror to the lens (set by the selection of the optical path length between the input and output wavefronts). As a consequence of this difference, as will be explained next, the lens on the more compact design is slightly concave near the vertex, whereas the less compact one is fully convex.

Let us look at the four profiles (two mirrors and two lenses) of the two designs in Figure 5 that can be parameterized using the same parameter. In the design on the left in Figure 5, consider two points **A′** and **A** on the mirror and the lens, respectively, and their symmetric points **B′** and **B** with respect to the symmetry axis (Figure 6). The mirror profile can be parameterized using the abscissa x of point **A′** in Figure 6 as a parameter. Then, we can associate each point **A** on the secondary with the point **A′** on the primary so that the étendue of the fraction of the input bundle impinging on the mirror segment **A′-B′** is equal to the étendue of the fraction output bundle that illuminates the receiver from the **A-B** line, that is:

$$E_{2D}=\iint_M dxdp=(2x)(2\sin\alpha)=2(b-a) \qquad (1)$$

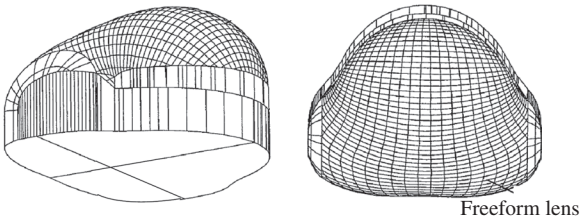

Figure 4 Freeform lens surface of the XR.

The last equality is given by the well-known Hottel formula [20] for the étendue of the rays illuminating the receiver of length L_C from the **A-B** line. This equality describes, for a given value of the x parameter, the equation of a hyperbola with foci at the edges of the receiver and passing through point **A** (drawn in blue in the insert in Figure 6). This hyperbola is a flow line of the exit bundle [21].

The dashed line joining **A′** and **A** in Figure 6 indicates the point-to-point mapping given between the mirror and the lens by the equi-étendue condition Eq. (1). This gives the common parameterization of the two profiles of the design on the left in Figure 5. The dashed line does not coincide with a ray trajectory; however, it is not far from it: it does become a ray trajectory in the aplanatic limit [22], which is obtained when both α and L_C tend towards zero, with $L_C/\sin\alpha$ = constant (this constant being the focal length of the aplanat). As a consequence, the slope of the lens at point **A** can be deduced approximately from Snell's law with the dashed line as an input ray and the tangent to the hyperbola (which bisects the two edge rays through A [21]).

Considering now the same value x of the parameter for both designs in Figure 5, the common parameterization for the four profiles is then obtained. Figure 7 highlights the

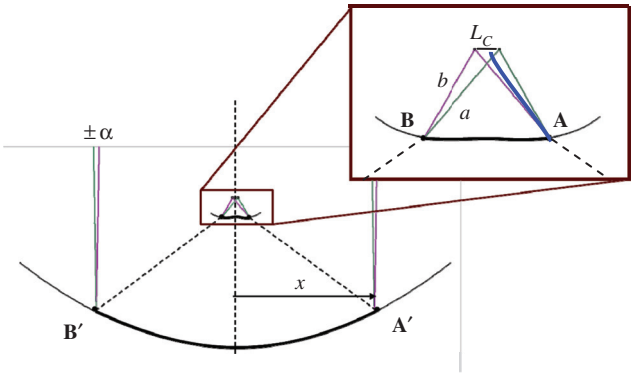

Figure 6 Common parameterization of the mirror and lens in the 2D XR design.

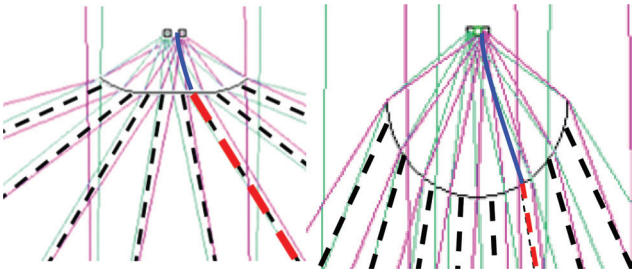

Figure 7 The red dashed lines indicate the common parameterization of the four surface profiles of the designs in Figure 5 for the parameter value $x=L_E/8$.

dashed lines associated with $x=L_E/8$ for the two designs in Figure 5 in red. The two red dashed lines connect to the same blue hyperbola defined in Eq. (1) but at two different points. Because the distance between the mirror and the lens is much larger in the design on the right, and both dashed red lines come from the same abscissa x at their respective mirrors, the red dashed line on the right is closer to the vertical than the one on the left. However, the slope of the tangent to the blue hyperbolas is very similar (both points are not far from the hyperbola asymptote). As a consequence, through the approximate application of Snell's law for the red dashed line to the blue hyperbola deflection, it is deduced that the lens on the right is sufficiently convex to produce such a deflection, whereas the one on the left is even slightly concave on axis to do so.

The shape of the SMS 3D lens in Figure 4 is intimately related to the aforementioned 2D reasoning. To deduce such a relationship formally, it is necessary to define a biparametric bundle associated with the SMS spines and use the proper étendue calculations in 3D space, which is done in the following sections.

3.1 Bundle of rays through spine pairs

From each point of the seed rib, using the blue and red wavefronts in Figure 1, the SMS 3D method builds paired SMS spines on the lens and on the mirror, as shown in Figure 3. Consider the bundle of rays M defined by those that, at each point on the mirror spine, pass through the lens spine between the two SMS edge rays (blue and red). That ray fan is shown in yellow for the central point of one mirror spine in Figure 8. That bundle M is biparametric, because any ray is defined by the two points of intersection with the spines, and those are defined by one parameter on each line. That bundle contains the two one-parametric subsets of rays of the SMS constructions, drawn as red and blue rays in Figures 3 and 8.

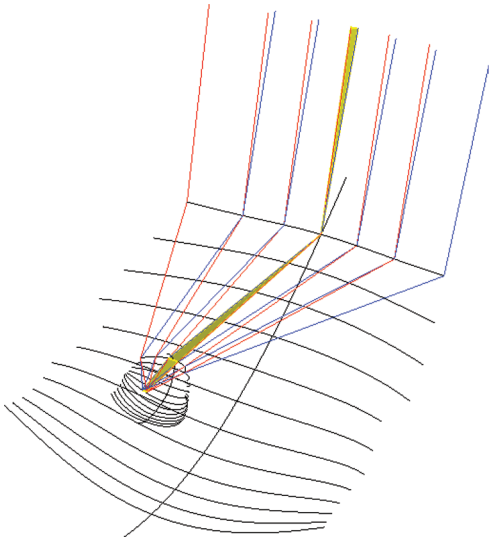

Figure 8 The yellow ray fan passes through the points on the lens spine in between the red and blue SMS edge rays.

For four-parametric ray bundles in 3D, the theorem of conservation of the étendue states that this is an invariant of the ray bundle when it is propagated through an optical system. In differential form, it is given by $dxdydpdq+dydzdqdr+dxdzdpdr$. This étendue is one of Poincaré's invariants, and this theorem is equivalent to Liouville's theorem in three dimensions. There exists another lesser-known étendue in 3D that is defined for biparametric ray bundles in 3D (not necessarily coplanar). This 2D étendue is given by:

$$E_{2D}=\iint_M dxdp+dydq+dzdr=\iint_M d\mathbf{v}\cdot d\mathbf{r} \tag{2}$$

This second invariant is another of Poincaré's invariants and it is equivalent to Lagrange's invariant. When the rays of the bundle are coplanar, it is also equivalent to Liouville's theorem in two dimensions, and it is just the first equality in Eq. (1).

We are interested in calculating Eq. (2) along a spine, so we will compute the interval $[\mathbf{v}_1, \mathbf{v}_2]$ of integration in $d\mathbf{v}$ for each point $\mathbf{r}$ of the spine to obtain:

$$E_{2D}=\iint \mathrm{d}\mathbf{v}\cdot d\mathbf{r}=\int(\mathbf{v}_2-\mathbf{v}_1)\cdot d\mathbf{r} \tag{3}$$

3.2 Common parameterization of the SMS spines

To find the common parameterization of the mirror and lens spines, equivalent to that expressed by Eq. (1) for the

2D case, we will calculate the étendue E_{2D} of the bundle defined in 3.1 for a segment of the spine symmetric with respect to the symmetry plane. We will perform the calculation at both the input and output side, and equating both étendues will lead to the expression equivalent to Eq. (1).

Consider first the calculation of E_{2D} at the input side along the mirror spine between points **B′** and **A′** (Figure 9). Because in this case the edge ray vectors $\mathbf{v}_1$ and $\mathbf{v}_2$ are constant (independent of **r**), and $\mathbf{v}_1\text{-}\mathbf{v}_2 = 2\sin\alpha\hat{\mathbf{x}}$, we deduce:

$$E_{2D} = \int_{B'}^{A'} (2\sin\alpha)\hat{\mathbf{x}}\cdot d\mathbf{r} = (2\sin\alpha)(2x) \tag{4}$$

where x is half the projected length of the mirror spine in the x-axis direction. Eq. (4) coincides exactly with the second equality in Eq. (2). Thus, we have found that it is a general formula, even though the mirror spine and the rays are not contained in a plane (which occurs in the 2D case).

Secondly, consider the calculation at the output side along the corresponding lens spine between points **B** and **A** (Figure 10). For this case, consider the eikonal functions [12] Ψ_1 and Ψ_2 associated with the spherical wavefronts converging to red and blue points, respectively. Then the edge ray vectors $\mathbf{v}_1$ and $\mathbf{v}_2$ (on the left of Figure 10) vary with **r** but can be computed as $\mathbf{v}_1 = \nabla\Psi_1$ and $\mathbf{v}_2 = \nabla\Psi_2$ [12]. Therefore, and

$$\begin{aligned} E_{2D} &= \int_{B}^{A} (\nabla\Psi_1 - \nabla\Psi_2)\cdot d\mathbf{r} \\ &= (\Psi_1(\mathbf{B}) - \Psi_1(\mathbf{A})) - (\Psi_2(\mathbf{B}) - \Psi_2(\mathbf{A})) \\ &= 2(b-a) \end{aligned} \tag{5}$$

where we have used the gradient theorem [23] and dimensions a and b are those indicated on the right-hand side of Figure 10. As occurred at the input side, Eq. (4) coincides exactly with the third equality in Eq. (2). Thus, we have also found that the Hottel formula is a general formula, even though the lens spine and the rays are not contained in a plane.

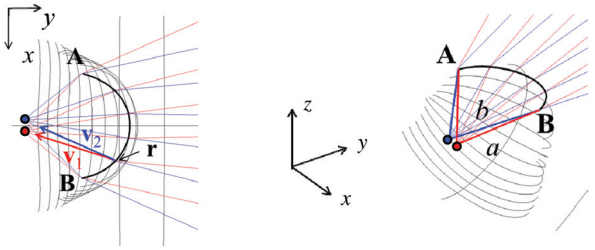

Figure 10 Calculation of the étendue of the biparametric bundle on the lens spine segment **A**-**B**.

3.3 Visualization

Because Eqs. (4) and (5) lead to exactly the same expression in Eq. (1), this allows the common parameterization of mirror and lens spine pairs with parameter x to be defined, as we did for the 2D case in section 2. Therefore, the qualitative conclusions on the convexity and concavity of the 2D lens profiles in Figure 7 can also be extrapolated to the 3D shapes of the spines.

Figure 11 highlights two of these pairs of spines, one pair in blue, close to the top rim of the mirror, and the other pair in red close to the bottom. The shape of the freeform lens in Figure 4 is then revealed: the lens is flatter close to the red spine than to its blue spine, because the distance between the red spines in the lens and the mirror is smaller than that of the blue spines.

Therefore, the étendue conservation has provided us with clues about how the spines evolve in a 3D space. However, this information is only partial. At the entry side only the projected length of the mirror spine on the x-axis

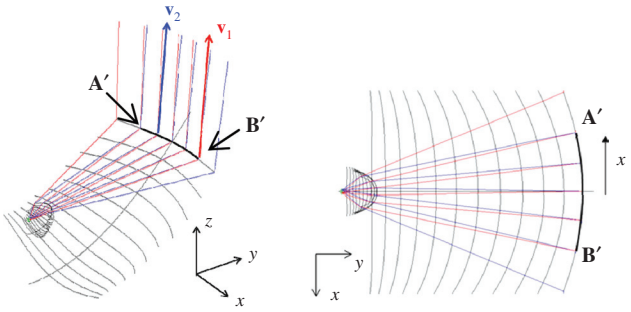

Figure 9 Calculation of the étendue of the biparametric bundle on the mirror spine segment **A′**-**B′**.

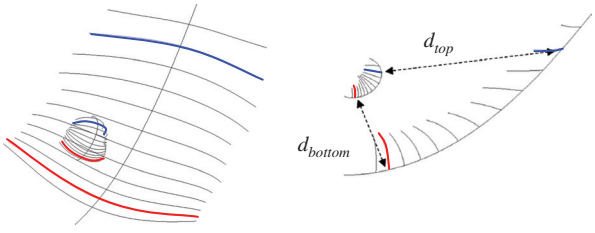

Figure 11 The lens is flatter close to the red spine than to its blue spine, because the distance between the red spines in the lens and the mirror is smaller than that of the blue spines ($d_{bottom} << d_{top}$).

is involved in Eq. (4), so the étendue does not give us any information as to how long the y or z projections of the mirror spine will be. By contrast, Eq. (4) only indicates that the points A and B lay on two hyperboloids (obtained through revolving that shown in Figure 6 around the x-axis), but no further clue as to how the 3D shape of the lens spine is obtained.

4 Conclusions

The shape of the spines calculated in the SMS 3D method is not as arbitrary as they seem at first sight, but are partially governed by étendue considerations. This is a consequence of the conservation of the étendue of the biparametric bundle linking the associated spine pairs, the bundle that contains the two one-parametric sets of SMS design rays passing through them. As a consequence, the shape of a highly freeform lens of an asymmetric XR design, whose curvature varies noticeably, can be qualitatively deduced *a priori*.

Acknowledgments: The authors would like to thank the European Commission (SMETHODS: FP7-ICT-2009-7 Grant Agreement No. 288526, NGCPV: FP7-ENERGY.2011.1.1 Grant Agreement No. 283798), the Spanish Ministries (ENGINEERING METAMATERIALS: CSD2008-00066, SEM: TSI-020302-2010-65, PMEL: IPT-2011-1212-920000), SIGMAMODULOS: IPT-2011-1441-920000, SUPERRESOLUCION: TEC2011-24019, and UPM (Q090935C59) for the support given to the research activity of the UPM-Optics Engineering Group, making the present work possible.

Received May 20, 2013; accepted July 3, 2013

References

[1] J. Schaefer, in 'International Optical Design, Technical Digest (CD)' (Optical Society of America, 2006), paper ThB1.
[2] M. Thomas and M. Sander, in 'Improving Optical Free-Form Production', Photonics Spectra September 2006.
[3] J. Koshel, in 'Illumination Engineering: Design with Nonimaging Optics' (Wiley, IEEE Press, Hoboken, 2013).
[4] N. Shatz and J. Bortz, in 'Nonimaging Optics' (Academic Press, New York, 2005).
[5] W. Cassarly, 'Illumination merit functions', SPIE Optics and Photonics Conference, Proc. SPIE, 6670, Nonimaging Optics and Efficient Illumination Systems IV, September 2007.
[6] M. Nicholson, http://www.zemax.com/kb/articles/265/1/How-to-Perform-Freeform-Optical-Design/Page1.html, 2009.
[7] V. I. Oliker, in 'Trends in Nonlinear Analysis', Ed. by M. Kirkilionis, S. Kromker, R. Rannacher and F. Tomi (Springer-Verlag, Heidelberg, 2003) p. 193.
[8] H. Ries and J. Muschaweck, J. Opt. Soc. Am. A 19, 590 (2002).
[9] F. Fournier, W. Cassarly and J. Rolland, Proc. SPIE, 7423, 742302 (2009).
[10] www.lpi-llc.com.
[11] A. Bäuerle, A. Bruneton, R. Wester, J. Stollenwerk and P. Loosen, Opt. Express 20, 14477 (2012).
[12] O. N. Stravoudis, in 'The Optics of Rays, Wave Fronts and Caustics', Ed. H.S.W. Massey and K.A. Bueckner (Academic Press, New York, and London, 1972), pp. 97–102.
[13] R. K. Luneburg, in 'Mathematical Theory of Optics', (University of California Press, Berkeley and Los Angeles, 1964), pp. 129–138.
[14] T. Levi-Civita, Mat. Nat. 9, 185 and 237 (1900).
[15] P. Benítez, J. C. Miñano, J. Blen, R. Mohedano, J. Chaves, et al., Opt. Eng., 43, 1489 (2004).
[16] F. Duerr, P. Benítez, J. C. Miñano, Y. Meuret and H. Thienpont, Opt. Express 20, 10839–10846 (2012).
[17] F. Duerr, P. Benítez, J. C. Miñano, Y. Meuret and H. Thienpont, Proc. SPIE 8486, 848609 (2012).
[18] A. Cvetkovic, M. Hernández, P. Benítez, J. C. Miñano, J. Schwartz, et al. Proc. SPIE 7043, 70430E (2008).
[19] A. Cvetkovic, O. Dross, J. Chaves, P. Benitez, J. C. Miñano, et al., in 'International Optical Design Conference 2006', Chairs/Editors G. Groot Gregory, J. M. Howard, R. J. Koshel, SPIE-OSA 6342, 63420R-1 (Vancouver, British Columbia, 2006).
[20] H. Hottel, in 'Heat Transmission', Ed. by W. H. McAdams (McGraw-Hill, New York, 1954).
[21] R. Winston, W. T. Welford, J. Opt. Soc. Am. 69, 532–536 (1979).
[22] J. C. Miñano, P. Benítez, W. Lin, J. Infante, F. Muñoz, et al., Opt. Express, 17, 24036–24044 (2009).
[23] R. Williamson and H. Trotter, in 'Multivariable Mathematics, 4th Edition.' (Pearson Education, Inc., Torino, 2004).

Pablo Benítez received his PhD degree in Nonimaging Optics from the Technical University of Madrid (UPM) in 1998 and Bachelor degrees in Telecommunication Engineering from UPM and Mathematics from Complutense University of Madrid (UCM), both in 1993. He has been an Associate Professor at UPM since 1999. His area of research ranges from optical design to manufacturing and applications, mainly concentrating on photovoltaics and solid state lighting. He has co-authored the book 'Nonimaging Optics' (Elsevier, 2004). He is co-inventor of the SMS optical design method and in particular SMS 3D for freeform optics design and freeform Köhler array devices. He is an SPIE fellow since 2012.

Juan-Carlos Miñano has been involved in Nonimaging Optics since the 1980s, mainly applied to LED lighting, optoelectronics and photovoltaic solar energy. He developed the Poisson-Bracket and the SMS design methods. His work has progressed from theoretical development to the commercial product. He has published more than 50 journal papers, given more than 200 Congress presentations, obtained more than 40 patents and written several books. Since 1997, he is Professor at the Universidad Politécnica de Madrid, and since 2000 he also collaborates as a Senior Scientist in LPI. He is an SPIE fellow and in 2010 was awarded with the prestigious A.E. Conrady Award of the SPIE.

Julio Chaves received his PhD in physics from the Instituto Superior Técnico, Universidade Técnica de Lisboa, Portugal in 2002. Chaves did postgraduate work during 2002 at Universidad Politécnica de Madrid, and in 2003 he moved to California, CA, USA and joined LPI. In 2006, he moved back to Madrid, Spain, and since then has been working with LPI-Europe. Chaves is the author of the book 'Introduction to Nonimaging Optics' and is the main author of the chapter on 'Solar concentrators' in the book 'Illumination Engineering: Design with Nonimaging Optics'. He has developed several new concepts, such as stepped flow-line optics, ideal light confinement by caustics, new Fresnel solar concentrators for multiple receivers, among others. He was the co-inventor of several patents and the co-author of many papers in the field of Nonimaging Optics. He also participated in the early development of the simultaneous multiple surface design method in three-dimensional geometry.

Asunción Santamaría received her Telecommunication Engineering degree from the Technical University of Madrid (UPM) in 1989, and her PhD degree in 1994 from the same University. She is Associate Professor at UPM-Telecommunication School since 1995. She has participated in more than 60 R&D projects (leading 30 of them), several of them belonging to the European Commission ESPRIT and ICT programs and to the European Space Agency. She is author or co-author of more than 25 scientific papers and books and more than 45 conference papers. She has been a member of the Technical Reviewers Staff of IEEE and ASTED journals and conferences and a member of the Technical Reviewers Committee of Spanish National R&D Programs. Since 2005, she is the Director of CeDInt-UPM R&D Center. She is an IEEE Communications Society Member.